Rocky Worlds DDT: JWST Data Analysis Report for TOI-771 b

Misty Cracraft, Tyler Baines, and Taylor J. Bell
JWST Data Analysis Team

June 26, 2026

1 Observation Overview

Under the RWDDT program, JWST-DDT-12656 Observation 1 obtained time-series imaging of TOI-771 b using MIRI/F1500W with the BRIGHTSKY subarray, covering 4.77 hours with the goal of measuring the secondary eclipse of the planet. The high-level science products (HLSPs) generated by our analyses are hosted on MAST and include both intermediate and final results to help drive research-community engagement.

We measured both the centroid position and width of the target's point-spread function (PSF) during each integration. The telescope pointing remained stable along the x and y axes throughout the observation after an initial settling time, while the width of the PSF along both axes increased smoothly during the first $\sim$1 hour of the observation before settling to a mostly stable value (see Figure 1) with a continuing slight rise.

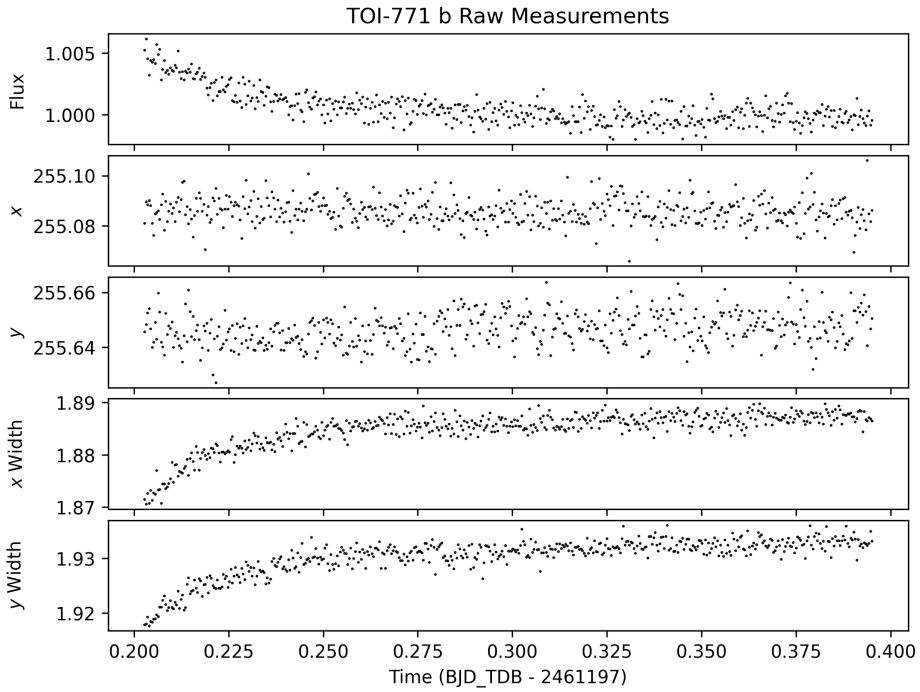

Figure 1: Measured flux and target centroid properties Time series of the relative changes in the normalized raw flux, centroid position (x, y), and PSF width (computed as the Gaussian standard deviation along the x and y axes), illustrating the initial settling behavior and overall stability of the telescope pointing and the PSF shape.

2 Data Reduction

This report presents results from two reductions and analyses performed by Analyst A (Cracraft) and Analyst B (Baines). Both analyses used the standard JWST pipeline (`jwst` v1.20.2 with CRDS context jwst_1464.pmap) for detector-level calibrations. Stage 1 processing included running the following steps: `dq_init`, `emicorr`, `saturation`, `firstframe`, `lastframe`, `reset`, `linearity`, `rscd`, `dark_current`, `jump` (with the threshold increased from 4.0 to 8.0), and `ramp fitting`. In Stage 2 we ran `flat_field`, but we disabled the `photom` step as flux-calibrated data are not desired for time-series analyses.

Photometric extraction and light curve fitting were completed using Stages 3–5 of the `Eureka!` Python package (v1.4.dev106+g3a6724481). A time series was constructed for each pixel, and 5σ outliers (along with all `NaN` values) were replaced using bilinear interpolation over the nearest neighbors. Next, a center-of-mass centroid was calculated for each integration using the 'mgmc' method within `Eureka!`'s Stage 3. The position and width of the target's PSF along the x and y axes were measured in each integration using a 2D Gaussian fit (see Figure 1). These measurements were compiled into cotrending vectors that were subsequently used as independent variables in the systematics modeling.

Photometric light curves were extracted in Stage 3 of `Eureka!` using the `photutils` package with circular apertures and 'exact' edges, where pixels are weighted by the fraction of their area lying within the specified aperture. A range of aperture and background annulus radii were considered. Aperture radii ranged from 4–11 pixels, in 1-pixel steps. The inner radius of the background annulus varied from 14 to 26 pixels in 4-pixel steps, while the annulus width ranged from 10 to 30 pixels in 10-pixel steps. Photometric light curves were generated for each source aperture + background annulus pair. In Stage 4, both analysts chose to mask any integrations lying 3.5σ away from the rolling median using a boxcar filter with a width of 20 integrations.

3 Light Curve Fitting

The most obvious feature in all of the extracted light curves is the large ramp during the first $\sim$1 hour of the observation. Analyst A trimmed off the first 150 integrations, and removed any exponential function in their light curve fit. The final fit results used a combination of fits: batman_ecl, a polynomial, PSF centroid positions (x, y) and widths (sx, sy).

Often, modeling systematic noise using detrending vectors and simple temporal trends is not enough to remove time-dependent 'red' noise from the light curve. To test this, the light curves were fit both with and without the inclusion of a `celerite2` Gaussian Process (GP) with a Matérn-3/2 kernel as a function of time to model low-level red noise. Both analysts found no clear evidence for residual red noise after fitting, and the results with and without the use of GP were consistent, though the uncertainties were slightly higher with GP. To demonstrate the robustness of our results to the use or exclusion of a GP, Analyst A chose their without-GP fit as their fiducial result while Analyst B chose their with-GP fit as their fiducial result.

All priors for the astrophysical and systematic models for our fiducial fits are summarized in Table 1. Our model can be summarized as:

$$\mathrm{Model}(t) = E(t) * S(t),$$

where $E(t)$ is the batman eclipse model, and $S(t)$ is the composite systematic noise model, defined as

$$S(t) = P(t)R(t)Y\Big(y(t)\Big)X\Big(x(t)\Big)SY\Big(sy(t)\Big)SX\Big(sx(t)\Big), \tag{1}$$

where

$$P(t) = c_0 + c_1(t - \bar{t})$$

is a linear trend in time where $\bar{t}$ is the mean time, and

$$R(t) = 1 + r_0 \exp\Big(-r_1(t - t_{\mathrm{start}})\Big)$$

is an exponential ramp, with t_{start} defined as the time of the first integration. Analyst A did not include an exponential ramp in their fits, i.e., $r_0 = 0; R(t) = 1$. Each of Y, X, SY, SX are linear decorrelation functions defined similarly to each other as

$$Y\Big(y(t)\Big) = 1 + c_y\Big(y(t) - \overline{y}\Big)$$

where $(x(t), y(t))$ is the measured centroid position as a function of time, and $(sx(t), sy(t))$ is the PSF width along the x- and y-axes as a function of time, and $(\overline{x}, \overline{y})$ is the time-averaged centroid position, and $(\overline{sx}, \overline{sy})$ is the time-averaged PSF size. Lastly, we also included a white noise scaling factor, `scatter_mult`, as a multiplier to the photometric uncertainties estimated during the Stage 3 reduction.

All fits used the `dynesty` dynamic nested sampling algorithm. Dynamic nested sampling is typically preferred for complex or multi-modal posteriors, as it adaptively allocates live points to focus more efficiently on the regions of interest. It is generally more efficient for parameter estimation, especially when the posterior has sharp features or multiple peaks. Our sampling began with an initial 512 live points using the 'rwalk' sampling algorithm and the 'multi' bounds and an initial $d\log\mathcal{Z} < 0.01$ stopping criterion (where $\mathcal{Z}$ is the Bayesian evidence). This was then followed-up by iteratively adding batches of 256 live points with a 'pfrac' of 0.9 (favoring a precise posterior distribution over a precise Bayesian evidence) until the default stopping criterion was achieved.

3.1 Results & Discussion

Each of the two analysts chose their own criteria to determine their final preferred reduction and light curve fit. These final results from both analysts are shown in Table 2. Analyst A selected a few aperture radii that had the lowest median absolute deviation (MAD) values from the Stage 3 pipeline. Apertures larger than 4–6 had much larger MAD values, as well as larger eclipse depth uncertainties, so a set of parameters were chosen for further analysis. Apertures of 4 or 5 and background annuli ranging from 14 to 22 in steps of 4 with widths of 10 and 20 pixels were chosen to examine. A final aperture of 4 with annulus from 18 to 28 pixels was chosen because it met the following

Table 1: The astrophysical and systematic model priors for the fits assuming a circular orbit. Fixed astrophysical parameters are shown without uncertainties and are taken from the circular fit from CIT's orbit fitting efforts during observational scheduling. Gaussian priors are shown as $\mathcal{N}(\mu, \sigma)$ with mean μ and standard deviation σ, while Uniform priors are shown as $\mathcal{U}(l, u)$ with lower-limit l and upper-limit u.

Parameter	Prior
P	2.3260184 days
$t_{\rm sec}$	$\mathcal{N}(2\,458\,573.5815, 0.0015)$ $\mathrm{BJD_{TDB}}$
b	0.14
a/R_*	18.9
e	0
R_* †	0.232
$R_{\rm p}/R_*$	0.05369
$F_{\rm p}/F_*$	$\mathcal{N}(150, 500)$ ppm
c_0	$\mathcal{N}(0.999, 0.01)$
c_1	$\mathcal{N}(-0.0020.1)$
c_y	$\mathcal{N}(0.0, 0.5)$
c_x	$\mathcal{N}(0.0, 0.5)$
c_{sy}	$\mathcal{N}(0.0, 0.5)$
c_{sx}	$\mathcal{N}(0.0, 0.5)$
scatter_mult	$\mathcal{U}(0.8, 10)$

†The stellar radius is used to account for the difference in light travel time throughout the planet's orbit.

criteria: a lower eclipse depth uncertainty, a reduced chi-squared value near 1.0 and a lower scatter_mult value than others in the set. Analyst A's fit residuals had a standard deviation of ∼730 ppm while Analyst B had ∼740 ppm; these correspond to noise levels ∼20% above the stellar photon noise limit.

Fits made using a 'medium'-width Gaussian prior on the mid-eclipse time ($\sigma t_{sec} = 0.025$ d) gave very similar results as the narrower prior ($\sigma t_{sec} = 0.0015$ d) assuming a circular orbit, indicating that the data are appear to be able to strongly constrain the mid-eclipse time largely independently from the priors. Analyst A selected the narrow prior for their fiducial analysis, since there were few differences.

Table 2: Fiducial eclipse fit results for TOI-771 b.

	Eclipse Depth [ppm]	$t_{\rm sec}$ [$\mathrm{BJD_{TDB}}$]	Residual Std. Dev. [ppm]
Analyst A †	462^{+81}_{-88}	$2\,458\,573.58272^{+0.00063}_{-0.00083}$	730
Analyst B	422^{+86}_{-91}	$2\,458\,573.58251^{+0.00094}_{-0.0010}$	741

†Our fiducial analysis, whose final and intermediate data products are hosted on MAST as an HLSP.

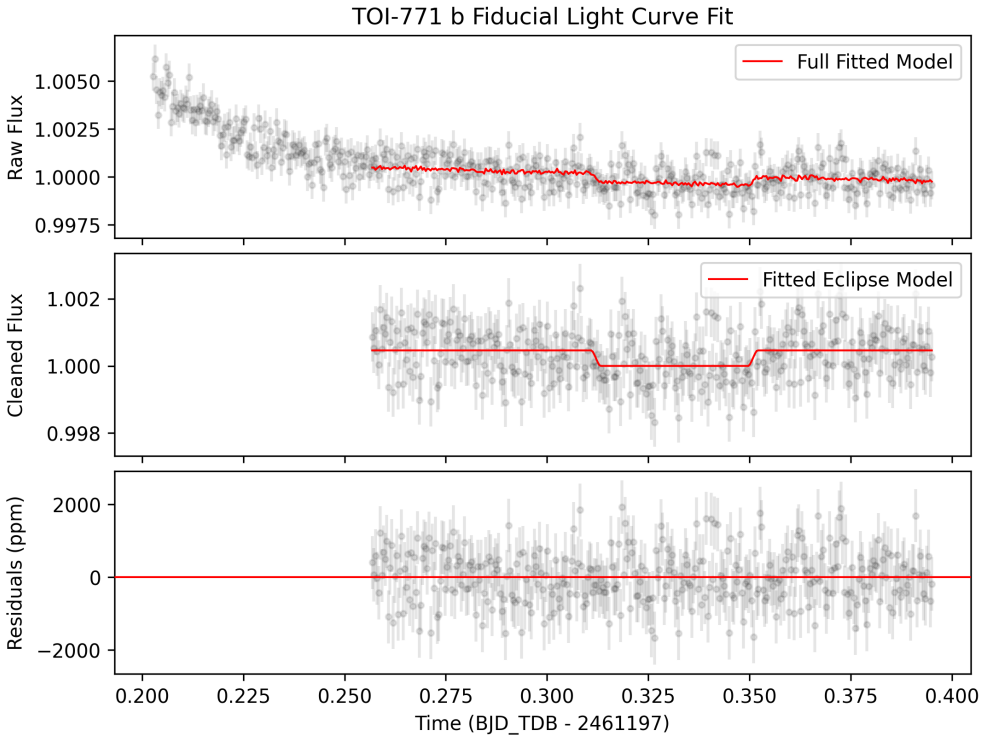

Figure 2: Fiducial light curve fit. *Top:* The raw, normalized flux measurements in black with the best fit combined systematics and eclipse model over-plotted in red. The first 150 integrations were not included in the fit. *Middle:* The systematics-divided flux measurements are shown in black, with the fitted eclipse model shown in red. *Bottom:* The "data − model" residuals.

4 Calibrated Stellar Flux Measurement

Following the methodology of Gordon et al. (2025), we measured absolutely-calibrated stellar photometry using `calints` FITS files with a 5.69 px aperture and an 8.63–11.45 px background annulus, applying an aperture correction of 1.497. Adding in quadrature the observational scatter with the $\sigma(\mathrm{CF}) = 0.48\%$ and $\sigma(\mathrm{repeat}) = 0.45\%$ terms from Gordon et al. (2025), we obtained a calibrated stellar flux of 3.842 ± 0.025 mJy.

5 Discussion and Outlook

This report provides a **snapshot** of TOI-771 b from a single observation. The relatively low uncertainties and consistent findings of an eclipse with multiple different tests are a good sign that the eclipse is roughly where it was expected to be, but the inclusion of additional eclipses is needed to more accurately constrain the eclipse depth and timing. For community analysts, the reduction/fitting configurations and noise benchmarks presented here offer a practical starting point; for modelers, the preliminary depths/timings and robust stellar flux measurements enable early exploration of different atmospheric and/or surface scenarios.